Wideband PPLN-Based Phase-Sensitively Amplified Transmission of 20-Channel 96-Gbaud WDM Signal

Shimpei Shimizu , *Member, IEEE*, Takayuki Kobayashi , *Member, IEEE*, Takushi Kazama ,
Takeshi Umeki , *Member, IEEE*, Masanori Nakamura , *Member, IEEE*, Koji Enbutsu , Ryoichi Kasahara ,
and Yutaka Miyamoto, *Member, IEEE*

Abstract—A periodically poled LiNbO$_3$ (PPLN)-based phase-sensitive amplifier (PSA) has the potential of ultra-low-noise and high-gain optical amplification. For the wideband operation of PSAs in optical fiber transmission, the chromatic dispersion (CD) that causes gain ripples is required to be compensated at the PSA input. We proposed a method to accurately estimate CD from the gain characteristic of a PSA. Estimated CD can be compensated by feed backing it to a spatial light modulator-based CD controller. This paper demonstrates a 2-THz wavelength-division multiplexing (WDM) single-span transmission using a PPLN-based PSA with CD pre-equalization based on our proposed method. The 20-channel WDM signal was modulated with single-polarized 96-Gbaud PS-64QAM, and its net data rate was 400 Gbps/channel. 2-THz signal bandwidth (4-THz bandwidth including an idler band) was the widest bandwidth in the fiber transmission using the PSA. We also discuss the system design of phase-sensitively amplified links for a high-symbol-rate and wideband WDM signal.

Index Terms—Chromatic dispersion, optical fiber communication, phase-sensitive amplification.

I. INTRODUCTION

FOR the demand on future client signals, the generation and transmission of a high-speed optical channel attracts much research attention in optical fiber transmission. Wavelength-division multiplexing (WDM) transmissions using 1-Tbps-class optical channels with higher-order and over-100-Gbaud modulation have been demonstrated [1], [2]. For higher-order modulation formats, high signal-to-noise ratio (SNR) is required. The SNR in optical fiber transmission is mainly defined by the propagation loss of the transmission fiber, launched optical power, and amplified spontaneous emission (ASE) noise from

optical amplifiers. Although an increase of the launched optical power improves optical SNR (OSNR), nonlinear optical effects in optical fibers such as the Ker effect become apparent with the high launched optical power. Self-phase modulation (SPM) and cross-phase modulation (XPM) caused by the Ker effect induce the nonlinear signal distortion, and the resulting received SNR is degraded in spite of OSNR improvement. Due to this launched power limitation, the noise figure (NF) improvement of optical amplifiers and fiber-nonlinearity mitigation are important research subjects for further enhancement of transmission throughput and reach. An erbium-doped fiber amplifier (EDFA) has been widely used in deployed WDM transmission systems. However, conventional amplifiers including an EDFA are classified as phase-insensitive amplifiers (PIAs), which have a 3-dB NF limit. The noise improvement of EDFAs has progressed to near this theoretical limit (e.g., [3]), and so there is not much room for improvement of the NF.

A phase-sensitive amplifier (PSA) based on optical parametric amplification (OPA) using highly nonlinear media has attracted research attention as an ultra-low-noise optical amplifier that breaks the theoretical NF limit of PIAs [4], [5]. In addition, the PSA can mitigate nonlinear signal distortion thanks to its phase regeneration effect [6], [7]. During the OPA process, a phase-conjugated light, namely idler light, is generated while amplifying the signal light. Coherent superposition between signal and idler light causes the phase-sensitive amplification. To amplify a WDM and higher-order quadrature-amplitude modulation (QAM) signal, a frequency-non-degenerate PSA (ND-PSA) can be used [5]–[9]. In the ND-PSA scheme, the idler light is generated on a transmitter side at a different frequency from the signal light beforehand and co-propagates through the transmission link with the signal light. The generation of the idler light can be performed by electrical [10] or optical methods [5]–[9]. The optical method using an optical phase conjugator (OPC) that utilizes OPA is effective for simultaneously generating the idler light of a wideband WDM signal. The idler light is converted to the same frequency as the signal light with phase-conjugation in the OPA process. When the phase and frequency relationship between the signal, idler, and pump light is optimal, the coherent superposition between the signal and idler light provides a gain of 6 dB in addition to the OPA gain. Thus, the effective NF limit of ND-PSAs reaches -3 dB for the signal band. Highly nonlinear fibers (HNLFs) and periodically poled LiNbO$_3$ (PPLN) waveguides are typically used as highly

efficient OPA media. PPLN-based OPA has the potential of a wideband, high-gain, and low NF [11]–[15].

A number of demonstrations for applying PSAs to optical communications have been reported with HNLF- and PPLN-based OPAs [5]–[11]. Simultaneous WDM phase-sensitive amplification of 1.1 THz [16] and 1.6 THz [8] were shown using HNLFs and PPLNs, respectively. Although the OPA has a wide-amplification bandwidth, the phase-sensitive amplification bandwidth is limited due to the chromatic dispersion (CD) generated with fiber propagation that causes a gain ripple for PSAs [17]. For optimal coherent superposition for all signal-idler pairs in a WDM signal, the relative phase must be uniform over the entire band. Therefore, the CD that causes the relative phase difference must be compensated at the PSA input. In the aforementioned demonstrations, a dispersion-managed link with a reverse-dispersion fiber (RDF) and a dispersion-compensation module (DCM) were utilized. To achieve further wideband phase-sensitive amplification, it is necessary to measure and compensate for any slight residual CD left on the transmission link.

We proposed a method to accurately estimate CD from the gain characteristic of PSA and experimentally showed a proof of concept [18]. Recently, an 80-km single-span transmission of a 2-THz WDM signal with the PPLN-based PSA supported by our proposed method was reported as a demonstration of the widest-band simultaneous phase-sensitive amplification [19]. The 20-channel WDM signal was modulated with 96-Gbaud probabilistically shaped (PS-) 64QAM, and its net data rate was 400 Gbps/channel. An 8-Tbps total throughput was achieved, and it was the first application of 100-Gbaud-class WDM signal for the PSA. This paper describes the details of our work [19]. We discuss the design of the single-span transmission system with phase-sensitive amplification of high-speed channels and a wideband WDM signal.

II. System Design for Phase-Sensitive Amplification of Wideband and High-Symbol-Rate WDM Signal

Fig. 1 shows a single-span transmission system with the OPC-PSA scheme. An OPC using OPA can simultaneous generate the idler light of each WDM channel with a single pump light. In the OPC stage, the gain from OPA is generated at the same time as the idler generation, so it can also work as a post-amplifier. If the output of OPA is less than the required fiber-launched power, additional amplification can be performed using other optical amplifiers in the OPC stage. The pump light in the PSA stage needs to be synchronized with the carrier component of each signal-idler pair. The signal-idler pairs generated by an OPA-based OPC have a common carrier component derived from the shared pump light. Therefore, the pump light used in the PSA stage should be synchronized with that used in the OPC stage. To synchronize the pump light, some techniques such as an optical injection locking (OIL) with a pilot light [20] or an optical phase-locking loop (PLL) with carrier recovery using sum-frequency generation [21] have been proposed. To achieve the wideband coherent superposition between signal-idler pairs, DCM accurately compensates for the CD. In addition, relative
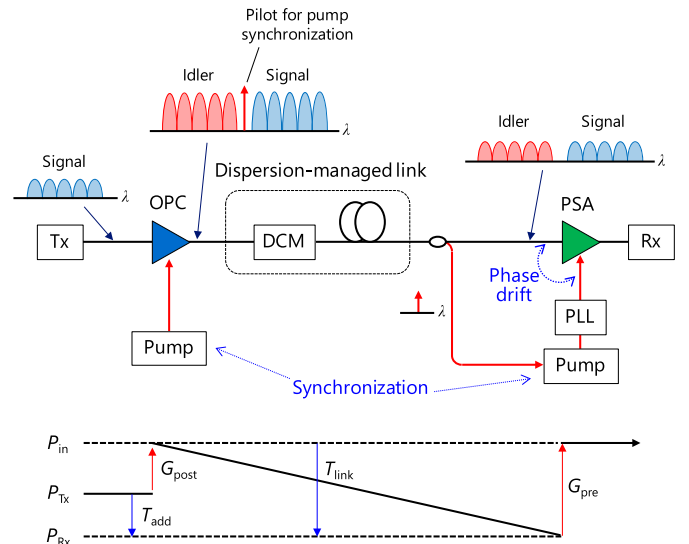

Fig. 1. Schematic and power diagrams of OPC-PSA scheme using optical injection locking with pilot light for pump synchronization. P_{in}, P_{Tx}, and P_{Rx} indicate link-launched power, input power to post-amplifier, and input power to pre-amplifier, respectively. G_{post} indicates gain of post-amplifier including OPC in transmitter side. T_{link} indicates transmission loss in dispersion-managed link. G_{pre} indicates gain of pre-amplifier including PSA in receiver side. T_{add} indicates additional attenuation from P_{Tx} due to T_{link} and determines the amount of noise decorrelation.

phase drift between the signal carrier and synchronized pump light must be compensated using a PLL with a phase shifter such as a piezoelectric transducer-based fiber stretcher (PZT) for stable coherent superposition between the signal-idler pairs.

This section describes the system design strategy for the phase-sensitive amplification of a high-symbol-rate and wideband signal using the OPC-PSA scheme. We clarify the application range of a PSA as an ultra-low-noise amplifier with respect to symbol rate and achievable information rate (AIR). Also, with numerical simulations, we investigate the impact of accuracy of a dispersion-managed link and the frequency resolution of a precise DCM on amplified signal quality.

A. Noise Decorrelation for High-Symbol-Rate Signal

Fig. 1 shows the transition of optical signal power in the transmission system. In a single-span transmission using a phase-sensitive pre-amplifier, a fiber loss design is important for directly reflecting the low-noise property of the PSA in improving the received signal quality [22]. The noise generated in the transmitter has a correlation between the signal and idler light. Such correlated noise is phase-sensitively amplified with the PSA in the same way as with the signal light. To take advantage of the phase-sensitive pre-amplifier, the noise decorrelation that sufficiently attenuates the correlated noise is required.

Assuming that the launched optical power per frequency required to achieve a certain spectral efficiency is P_f, the launched channel power with a symbol rate of B is expressed as

$$P_{in} = B \cdot P_f \tag{1}$$

A gain of a post-amplifier at the transmitter required to achieve this optical power is expressed as

$$G_{\text{post}} = \frac{P_{\text{in}}}{P_{\text{Tx}}} \qquad (2)$$

where P_{Tx} is the minimum power before post-amplification. The minimum power is mainly determined by the output power of a continuous wave (CW) light source and loss of an optical modulator. For the OPC-PSA scheme, G_{post} also includes a gain of the OPC. The average power per frequency of the ASE noise output from the post-amplifier part is expressed as

$$N_{\text{post}} = \alpha_{\text{post}} \left(G_{\text{post}} - 1 \right) h\nu \qquad (3)$$

where α_{post} is the NF of the post-amplifier, h is a Plank constant, and ν is a frequency. After fiber transmission and pre-amplification, ASE noise per frequency is expressed as

$$N_{\text{total}} = G_{\text{pre}} T_{\text{link}} \alpha_{\text{post}} \left(G_{\text{post}} - 1 \right) h\nu + \alpha_{\text{pre}} \left(G_{\text{pre}} - 1 \right) h\nu \qquad (4)$$

where G_{pre} is the gain of the pre-amplifier, T_{link} is the propagation loss of a transmission link, and α_{pre} is the NF of the pre-amplifier. The ratio of the total ASE noise between two cases of pre-amplification by PSA and that by PIA is

$$N_{\text{ratio}} = \frac{G_{\text{pre}} T_{\text{link}} \alpha_{\text{post}} \left(G_{\text{post}} - 1 \right) + \alpha_{\text{PSA}} \left(G_{\text{pre}} - 1 \right)}{G_{\text{pre}} T_{\text{link}} \alpha_{\text{post}} \left(G_{\text{post}} - 1 \right) + \alpha_{\text{PIA}} \left(G_{\text{pre}} - 1 \right)} \qquad (5)$$

where α_{PSA} and α_{PIA} are the NF of PSA and PIA, respectively. For simplicity, assuming that $G_{\text{pre}} = T_{\text{link}}^{-1}$ and $\alpha_{\text{post}} = \alpha_{\text{PIA}}$,

$$N_{\text{ratio}} = \frac{\alpha_{\text{PIA}} \left(G_{\text{post}} - 1 \right) + \alpha_{\text{PSA}} \left(G_{\text{pre}} - 1 \right)}{\alpha_{\text{PIA}} \left(G_{\text{post}} - 1 \right) + \alpha_{\text{PIA}} \left(G_{\text{pre}} - 1 \right)} \qquad (6)$$

N_{ratio} also represents the amount of improvement in effective NF when PIA is replaced with PSA. Thus, the effective NF of PSA used as a pre-amplifier is expressed as

$$\alpha_{\text{eff}} = \frac{\alpha_{\text{PIA}} \left(G_{\text{post}} - 1 \right) + \alpha_{\text{PSA}} \left(G_{\text{pre}} - 1 \right)}{\alpha_{\text{PIA}} \left(G_{\text{post}} - 1 \right) + \alpha_{\text{PIA}} \left(G_{\text{pre}} - 1 \right)} \cdot \alpha_{\text{PIA}} \qquad (7)$$

It can be seen that the effect of PSA on the received signal requires a sufficiently large loss, that is, long propagation distance, in the transmission link. The effective NF of PSA can be estimated quantitatively by using the additional attenuation from P_{Tx} contained in T_{link}, which is defined as

$$T_{\text{add}} \equiv \frac{G_{\text{post}}}{G_{\text{pre}}}$$
$$= \frac{B \cdot P_{\text{f}} \cdot T_{\text{link}}}{P_{\text{Tx}}} \qquad (8)$$

Namely, T_{add} represents the ratio of received signal power via the transmission link to P_{Tx}. Using T_{add}, α_{eff} is expressed as

$$\alpha_{\text{eff}} \approx \frac{\alpha_{\text{PIA}} + \alpha_{\text{PSA}} \cdot T_{\text{add}}^{-1}}{\alpha_{\text{PIA}} + \alpha_{\text{PIA}} \cdot T_{\text{add}}^{-1}} \cdot \alpha_{\text{PIA}} \quad \text{when } G_{\text{post}}, G_{\text{pre}} \gg 1 \quad (9)$$

Figure 2 shows the effective NF of PSA as a function of T_{add}^{-1} assuming ideal noise performance of amplifiers that $\alpha_{\text{PIA}} = 3$ dB and $\alpha_{\text{PSA}} = -3$ dB. With an additional attenuation of 20 dB, sufficient noise decorrelation is performed, and an effective NF
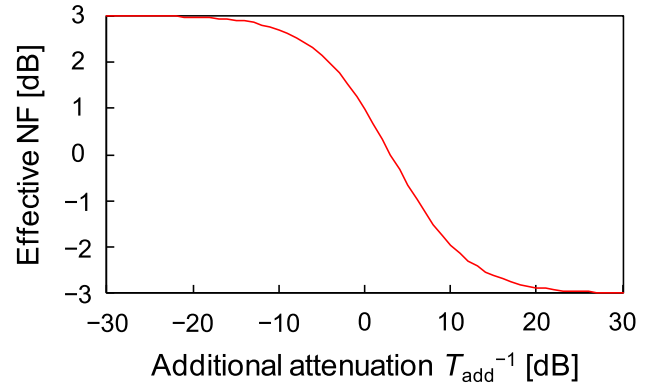

Fig. 2. Effective NF of phase-sensitive pre-amplifier in single-span transmission system as a function of additional attenuation in transmission link.

of about -2.9 dB can be achieved. That is, it is suggested that PSA is effective on sufficiently long transmission links with a large transmission loss that satisfy $T_{\text{add}}^{-1} > 20$ dB. P_{f} is a parameter that depends on T_{link}, so there is a trade-off relationship between the spectral efficiency and T_{link}. The application range where a PSA is effective can be expanded if the G_{post} can be made small by increasing the minimum optical power in the transmitter; that is, a PSA will function effectively even with a small link loss (short propagation distance). However, there are limits for the output of the light source and the loss of the optical modulator. Therefore, as the symbol rate increases, the low received power per frequency is required for the noise decorrelation, and the application range of a PSA in spectral efficiency is limited. Fig. 3 shows an example of the application range of an ND-PSA in spectral efficiency. The symbol-rate dependence of AIR is calculated assuming $T_{\text{add}}^{-1} = 20$ dB, where a PSA operates with sufficiently low noise. The minimum power in the transmitter determines the SNR of the received signal at $T_{\text{add}}^{-1} = 20$ dB. α_{PIA} and α_{PSA} were set to 4.5 dB, and -1.5 dB. It is assumed that the noise of the received signal is sufficiently dominated by the ASE noise from the pre-amplifier (i.e., the PSA in Fig. 1), and thus, AIR was calculated as

$$AIR = \log_2 \left(1 + \frac{T_{\text{add}} \cdot P_{\text{Tx}}}{\alpha h\nu B} \right) \qquad (10)$$

where α is the NF of the pre-amplifier. For a polarization-division multiplexing (PDM) signal, AIR was also calculated as

$$AIR_{\text{PDM}} = 2\log_2 \left(1 + \frac{T_{\text{add}} \cdot P_{\text{Tx}}}{2\alpha h\nu B} \right) \qquad (11)$$

The higher the symbol rate of the signal, the narrower the range of the information rate of the signal in which low-noise property of PSAs is effective. To expand the application range of PSAs for channel throughput, a high-power light source and a low-loss optical modulator are important technologies.
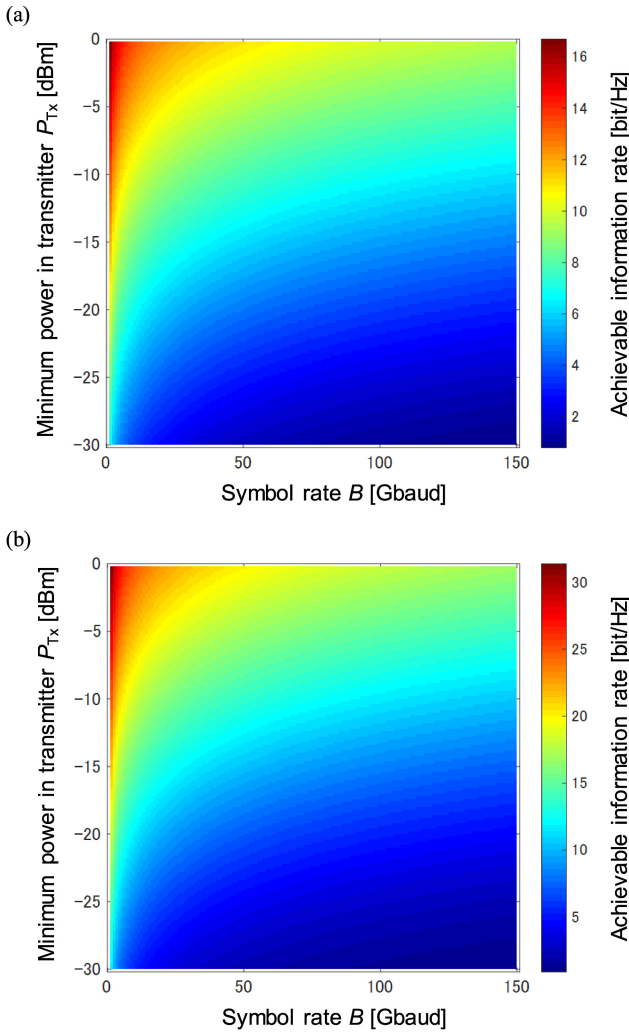
(a)

(b)

Fig. 3.   Maximum achievable information rate (AIR) assuming $T_{\mathrm{add}}^{-1} =$ 20 dB as functions of minimum power in transmitter and symbol rate (a) for single-polarized signal and (b) for polarization-division multiplexed signal.

B. Impact of Resolution in Residual CD Compensation on Wideband Signal

The gain spectrum of a PSA depends on the amount of CD in the transmission link. The CD causes the phase difference between the signal and idler light, resulting in a gain ripple. Therefore, in the phase-sensitively amplified link, dispersion management is required. A fiber Bragg grating (FBG) and an RDF are effective for wideband analog CD compensation. However, a simultaneous wideband CD compensation by the FBG causes phase ripples that prevent a broad coherent superposition between a signal-idler pair. Wideband precise CD compensation including higher-order CDs is difficult for the RDF. In addition, although one of the operational requirements of the PSA link is the ability to handle slight changes in the CD (e.g., caused by the connection of fiber-patch codes and changes in environmental temperature), adaptive and precise CD compensation using these methods is difficult. A spectral shaper using a spatial light modulator (SLM), such as a wavelength selective switch, can adaptively and precisely control the CD over a wideband [23],

and a PSA link configuration that accurately measures the slight residual CD and compensates for it with an SLM have been proposed [18]. Because the control range of a CD is limited by the frequency resolution and the modulation depth of the SLM, large CDs must be roughly compensated using RDF or FBG apart from the compensation by the SLM. The SLM compensates for the slight residual CD including higher-order characteristics of the rough compensation. However, the compensation of the residual CD by the SLM is discrete and includes a quantization error. The farther the signal-idler pair is from the center frequency, the greater the effect of the quantized CD compensation. We investigate the impact of the resolution of an SLM and the amount of the discrete compensation on signal quality after phase-sensitive amplification.

The gain of PSAs depends on the relative phase relationship between the signal and pump light [24]:

$$G = G_{\mathrm{I}}\cos^2\left(\Delta\phi\right) + \frac{1}{G_{\mathrm{I}}}\sin^2\left(\Delta\phi\right) \tag{12}$$

where $\Delta\phi$ is the phase difference between the signal and pump light and G_{I} is the gain of the in-phase component, which means the maximum gain of the PSA. When $\Delta\phi = n\pi$ ($n = \ldots, -1, 0, 1, \ldots$), the signal light is amplified with $G = G_{\mathrm{I}}$. When $\Delta\phi = n\pi/2$, the signal light is de-amplified with $G = 1/G_{\mathrm{I}}$. For the phase-sensitive signal amplification, $\Delta\phi$ is controlled using a PLL so that $G = G_{\mathrm{I}}$. With the residual CD, $\Delta\phi$ depends on frequency; that is, the gain spectrum is affected by a ripple as follows [17]:

$$G_{\mathrm{sp}}\left(f\right) = G_{\mathrm{I}}\cos^2\left[\Delta\phi\left(f\right)\right] + \frac{1}{G_{\mathrm{I}}}\sin^2\left[\Delta\phi\left(f\right)\right] \tag{13}$$

Considering up to the second-order term of CD, $\Delta\phi(f)$ is expressed as

$$\Delta\phi\left(f\right) = \frac{\pi D c}{f_0^2}\left(f - f_0\right)^2 \tag{14}$$

where D is the residual CD, c is the speed of light, and f_0 is the center frequency in the phase-matching of the amplification medium. In the ND-PSA, a PLL monitors an optical channel arranged at a different frequency from f_0. Because the frequency that serves as a reference for the relative phase is that monitored by the PLL, the gain spectrum is modified as follows [18]:

$$G_{\mathrm{sp}}\left(f\right) = G_{\mathrm{I}}\cos^2\left[\Delta\phi\left(f\right) - \theta\right] + \frac{1}{G_{\mathrm{I}}}\sin^2\left[\Delta\phi\left(f\right) - \theta\right] \tag{15}$$

$$\theta = \frac{\pi D c}{f_0^2}\left(f_0 - f_{\mathrm{PLL}}\right)^2 \tag{16}$$

where f_{PLL} is a frequency monitored by the PLL. According to Eq. (15), the CD produces a gain ripple. When an optical channel undergoes a gain ripple, the signal quality deteriorates due to a passband-narrowing-like effect [18].

When compensating for the CD using an SLM, the signal light is diffracted with a grating before irradiating an SLM. Then, an SLM performs phase modulation on each frequency component. An SLM typically has a square pixel structure, and the phase modulation for the signal light is quantized on the spectrum with a finite resolution. Because the relative phase
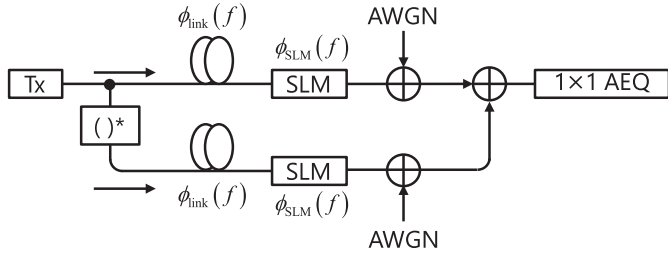
Fig. 4. Simulation model for investigating impact of SLM quantization error on signal quality after phase-sensitive amplification. $\phi_{\text{link}}(f)$ is the amount of phase modulation caused by residual CD in transmission link, $\phi_{\text{SLM}}(f)$ is the amount of phase modulation provided by SLM, and ( )$*$ indicates phase conjugation.

variation due to the CD becomes steep in the frequency component far from f_0, it is greatly affected by this quantization. The amount of residual CD after CD management with the fiber configuration is also an important parameter. The greater the contribution of the SLM in CD compensation, the greater the quantization error. We performed numerical simulations to investigate the impact of the frequency resolution of an SLM on signal quality. Fig. 4 shows the simulation model. The signal and idler light were calculated independently and were finally added together to simulate phase-sensitive amplification. f_0, which is the reference frequency for the phase difference due to CD, was set to 194.0 THz. The signal modulation formats were 32- or 96-Gbaud 16QAMs. The over sampling rate of the signal in the time domain was 4 sample/symbol. The frequency difference Δf between f_0 and the signal was set to 1 or 2 THz. The signal and idler light were arranged at $194.0 - \Delta f$ and $194.0 + \Delta f$, respectively, and were given the CD of D_{link} that simulated the residual CD in the dispersion-managed transmission link. The amount of phase modulation $\phi_{\text{link}}(f)$ caused by D_{link} was calculated on the basis of frequency arrangement. The phase modulation was applied in the Fourier domain by performing a fast Fourier transform on the time samples of the signal and idler light. Then, their CDs were compensated by the SLM. The amount of phase modulation provided by the SLM $\phi_{\text{SLM}}(f)$ was the quantized value of $-\phi_{\text{link}}(f)$ with a predetermined resolution. After the CD compensation, the signal and idler light were combined with additive white Gaussian noise (AWGN), respectively. The amount of AWGN was set so that the SNR after signal demodulation was ~16 dB when CD compensation was completely performed. Finally, the signal light was combined with the idler light, down-sampled to twice the symbol rate, and demodulated with a 1×1 adaptive equalizer (AEQ) updated by a decision-directed least-mean-square (DD-LMS) algorithm. The frequency resolution of the SLM was changed from 0 to 10 GHz in 0.1-GHz increments. The D_{link} in the transmission link was changed from 0 to 10 ps/nm in 0.2-ps/nm increments. The frequency step of analysis area in the Fourier domain was set to 0.1 MHz, regardless of symbol rates. The penalty for the signal quality due to the resolution in CD compensation and residual CD in a transmission link was evaluated by the SNR calculated from the variance of the signal constellations after demodulation. Only simulations with positive CDs were performed. The gain

spectrum with negative CDs is the same as those with positive CDs, and thus, the penalties are the same with the same absolute values.

Fig. 5 shows the simulation results indicating SNR penalty. It can be confirmed that the coarser the resolution of the SLM, the more accurately the analog CD management with the fiber configuration needs to be performed. In addition, the farther the channel was from f_0, that is, the wider the bandwidth of the WDM signal, the more accurate analog CD management was required. For channels with the same frequency arrangement, the contours of 0.2-dB penalty do not differ much depending on the symbol rate. Gain ripples do not always occur when a phase jump occurs due to the quantization error of the SLM. Because the impact of the phase jump on the gain spectrum were averaged for wider-band signals, the contours of 96-Gbaud signals were smoother than those of 32-Gbaud signals. This means that high-symbol-rate signals are robust to fluctuations of CD and a pump frequency. The resolution of the SLM we used in the transmission experiments in the next section was 1 GHz. For channels 1-THz away from f_0, the SNR penalty was ~0.1 dB even with a residual CD over 10 ps/nm. However, for channels 2-THz away from f_0, <7.0-ps/nm residual CD was required to suppress the SNR penalty within 0.2 dB. Residual CD should be sufficiently reduced using analog DCMs such as the RDF and FBG, on the basis of the acceptable SNR penalties.

III. 80-KM SINGLE-SPAN TRANSMISSION OF 20-CHANNEL 96-GBAUD WDM WITH 2-THZ PPLN-BASED PSA

To demonstrate the wideband phase-sensitive amplification with high-symbol-rate signals, we conducted an 80-km single-span transmission with a 20-channel 96-Gbaud WDM signal. We used PPLN waveguides as OPA media, which had an amplification bandwidth over 10 THz [11]. This section shows this demonstration based on the system design discussed in the previous section.

A. Experimental Setup

Fig. 6 shows the experimental setup for an 80-km single-span transmission using a PPLN-based ND-PSA with a 20-channel WDM signal. The WDM signal was modulated with 96-Gbaud single-polarized (SP-) PS-64QAM that has the same shaping factor as Ref. [1]. WDM channels were densely allocated in a 100-GHz grid from 191.95 to 193.95 THz (1545.72–1561.82 nm). The precise CD pre-compensation was performed by liquid-crystal on silicon (LCOS)-based SLM with a 1-GHz frequency resolution. The phase-matching frequency of our PPLN waveguides was 194.0 THz (1545.32 nm). OPA using PPLN waveguides requires a second-harmonic (SH) pump light. To obtain the strong second-harmonic pump light, it is effective to amplify the CW light at f_0 with C-band EDFA and then convert it with second-harmonic generation (SHG). We utilized a 2-stage configuration using different PPLN waveguides for SHG and OPA to suppress the parametric cross-talk [25]. The frequency synchronization of the pump light was conducted by an OIL using a co-transmitted pilot light.
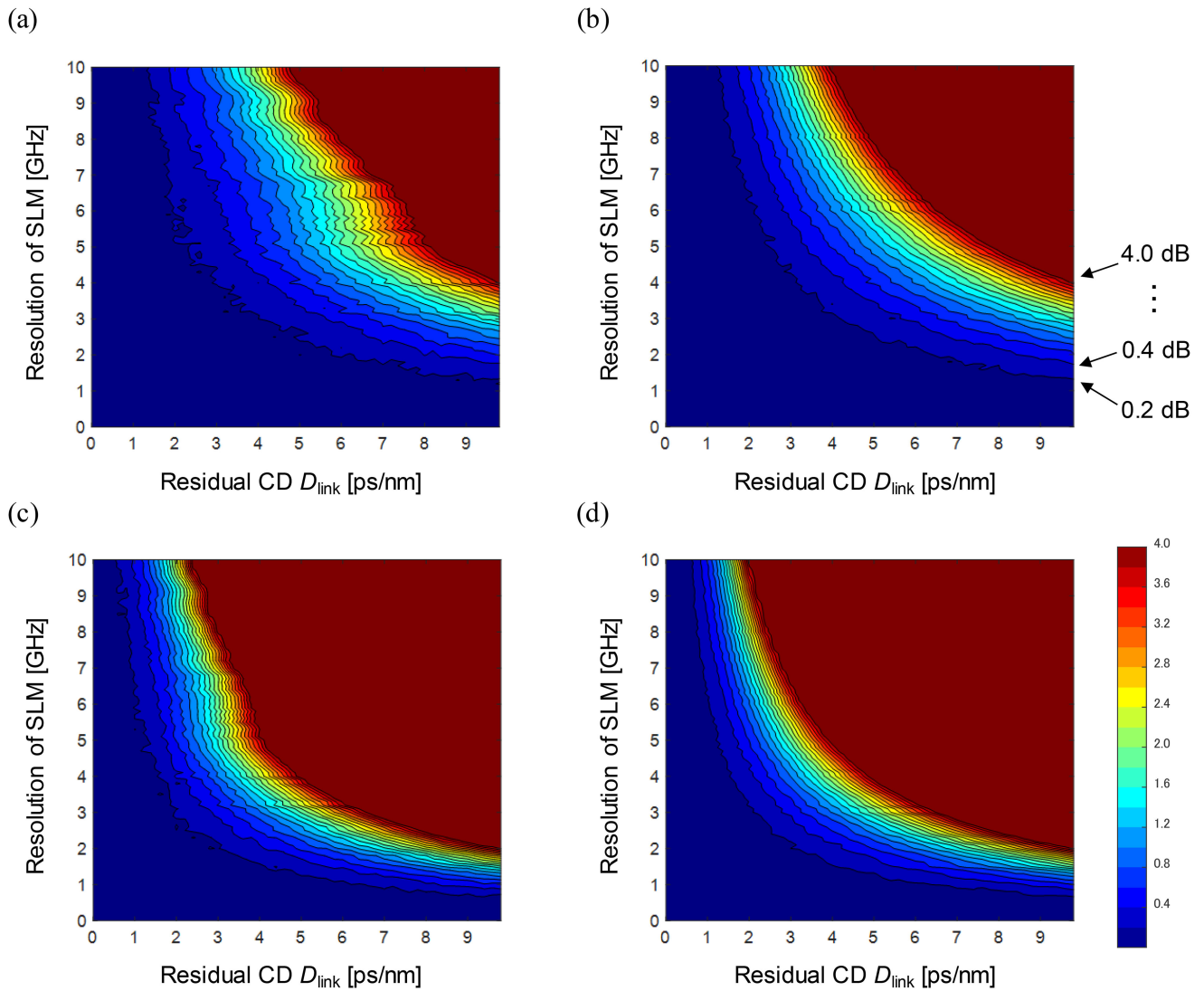
(a)

(b)

(c)

(d)

Fig. 5. SNR penalty versus resolution of SLM (vertical axis) and residual CD in transmission link (horizontal axis). Contours are drawn at 0.2-dB intervals. Filled area in upper right of each graph means a penalty of >4.0 dB. (a) 32-Gbaud 16QAM signal 1-THz away from f_0, (b) 96-Gbaud 16QAM signal 1-THz away from f_0, (c) 32-Gbaud 16QAM signal 2-THz away from f_0, and (d) 96-Gbaud 16QAM signal 2-THz away from f_0.
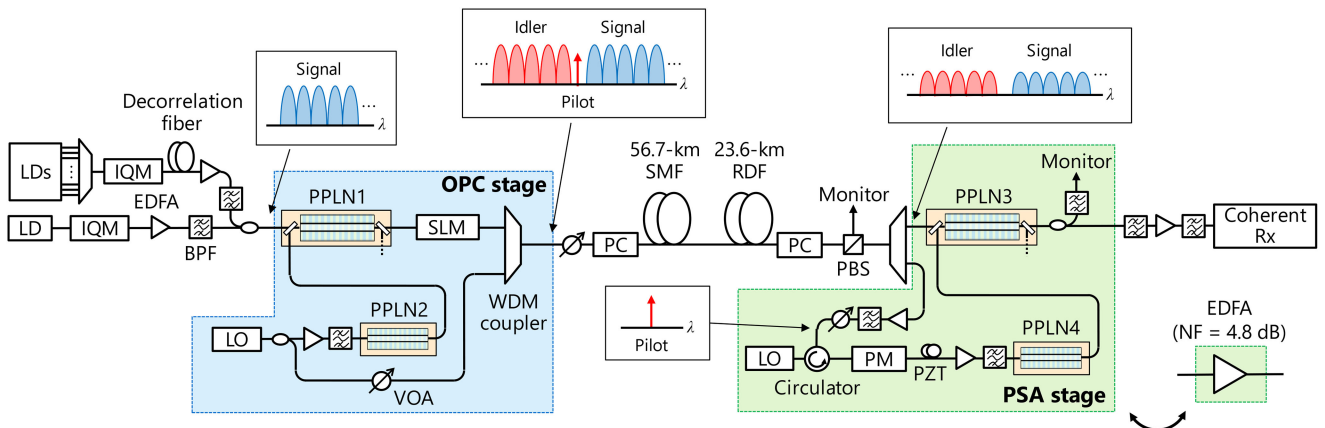

Fig. 6. Experimental setup of 80-km single-span transmission of 20-channel 96-Gbaud PS-64QAM signals with 2-THz PPLN-based PSA. The green frames represent the components used in the PSA and EDFA cases. LD: laser diode, IQM: I/Q modulator, SLM: spatial light modulator, LO: local oscillator, BPF: band-pass filter, VOA: variable optical attenuator, PC: polarization controller, PBS: polarization-beam splitter, PM: phase modulator, PZT: piezoelectric transducer-based fiber stretcher.
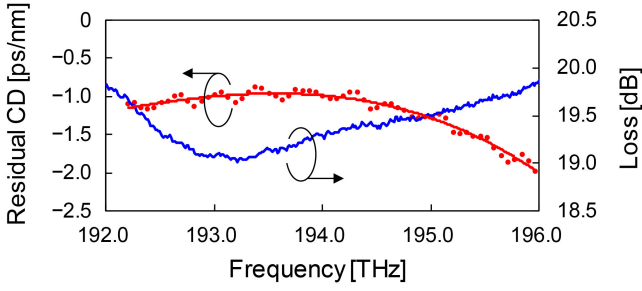
Fig. 7. Spectra of propagation loss and residual CD in 80-km dispersion-managed transmission link measured by dispersion analyzer. Plots indicate measured CD values and a line indicates polynomial approximation.

20 tunable lasers with 100-GHz spacing from 192.0 to 193.9 THz were used as the CW light sources of WDM interference channels. The interference channels were simultaneously modulated by an I/Q modulator (IQM) and decorrelated using a 20-km single mode fiber (SMF). For a channel under test (CUT), an external cavity laser (ECL) with a ∼10-kHz linewidth was used as a CW light source. The IQMs were driven by a 120-Gsample/s arbitrary waveform generator and modulated CW light with Nyquist-pulse-shaped 96-Gbaud PS-64QAM with a roll-off factor of 0.03. The minimum power of the CUT in the transmitter was −15 dBm at the output of the IQM. The CUT and the interference channels were combined by a 2 × 1 coupler. All channel measurements were conducted by sweeping the frequency of the ECL. The WDM signal was first input to the OPC stage for idler light generation. The signal-idler pairs were simultaneously generated by OPA with a gain of 12 dB using a single free-running pump light and then passed through the SLM for CD pre-compensation. The local oscillator (LO) driven at 194.0 THz with ∼5-kHz linewidth was divided using a 3-dB coupler as the pump light in the OPC stage and the pilot light for the OIL. The pump light was amplified by a C-band EDFA and then converted to a SH pump by the SHG. The pilot light was inserted into the WDM signal using a WDM coupler after the SLM.

The WDM signal and the pilot light was launched to an 80-km CD-managed transmission link at −14.3 dBm/channel and −18.0 dBm, respectively. The transmission link consisted of a 56.7-km SMF and a 23.6-km RDF. Before input to the pre-amplification stage (PSA/EDFA or EDFA/EDFA), only the transverse magnetic (TM) polarization component of the signal light was extracted with the polarization controllers (PCs) at both ends of the transmission link and a polarization-beam splitter (PBS) because PPLN waveguides have polarization sensitivity. The PCs were adjusted so that the optical power in the monitor port of the PBS was the lowest. Then, the pilot light was extracted using a WDM coupler. Fig. 7 shows frequency dependence of propagation loss and the CD of the dispersion-managed link as measured by a dispersion analyzer. The propagation loss of this link was from −20 to −19 dB. The difference in propagation loss between each signal-idler pair was pre-equalized in the SLM. To reflect the low-noise property of the PSA in the signal quality, it was necessary to set the PSA input power to be less than −35 dBm/channel assuming $T_{\text{add}}^{-1} = 20$ dB. Due to the loss of the transmission link and each component, the input power

of the PSA stage was <−35 dBm/channel The RDF widely compensated for the CD including higher-order terms, and the residual CD was from −2 to −1 ps/nm. From the discussion in Section II-B, a 1-GHz frequency resolution of the SLM can perform CD compensation without deterioration of signal quality over 2 THz.

In the PSA stage, the phase-sensitive amplification was performed using a frequency-stabilized pump light. The frequency stabilization was performed with the OIL using the pilot light. The pilot light was amplified by the polarization-maintaining EDFA and was input to the slave LO via an optical circulator at −15 dBm. The slave LO had a ∼800-kHz linewidth without the OIL. The relative phase drift between the signal and pump light was compensated by a PZT-based PLL (PZT-PLL). A phase modulator (PM) was used for modulating a 1-MHz dither signal for the PZT-PLL. The PZT-PLL monitored a 10% tapped channel at 193.5 THz as the locking frequency. The gain of the PSA stage was ∼20 dB for all channels. To evaluate the noise performance of the PSA, an experiment was conducted in which the PSA stage, shown in the green frame in Fig. 6 (after the WDM coupler), was replaced with an EDFA (typical NF = 4.8 dB) operating at the same gain as the PSA. In the EDFA case, we used the same transmitter configuration including the OPC stage as in the PSA case, except for the phase modulation in the SLM, although these are really not required. Under our experimental conditions, the noise from the pre-amplification was sufficiently dominant, so the noise from the OPC stage did not affect the noise performance. Note that, the WDM coupler was not needed for the EDFA case, and thus its loss (∼0.5 dB) was a disadvantage in the EDFA case.

The CUT was extracted after pre-amplification using PSA/EDFA or EDFA/EDFA. The extracted CUT was received by a dual-polarization coherent receiver consisting of an optical 90-degree hybrid and four 70-GHz balanced photodetectors. The input optical power of the CUT to the receiver was strong enough, so there was no performance degradation due to the polarization-diversity detection of a single-polarized signal. After digitization using a 200-Gsample/s digital storage oscilloscope, the received signal was demodulated in offline digital signal processing on the basis of complex 8 × 1 AEQ [1]. The AEQ was pre-converged with training symbols. The tracking mode of the AEQ utilized the DD-LMS algorithm and pilot-aided LMS algorithm using periodically inserted pilot symbols. The signal qualities were evaluated by calculating their normalized generalized mutual information (NGMI) and SNR on the basis of the variance of the signal from desired symbols. Fig. 8 shows the OSNR dependence of the SNR after the demodulation expressing saturation characteristics of Tx/Rx in back-to-back transmission. We assumed that the forward error correction (FEC) threshold of the NGMI was 0.857 with a net data rate of 404.72 Gbps/channel and a spectral efficiency of 4.2158 bit/Hz.

B. Precise CD Compensation

Fig. 9 shows the spectrum of the WDM signal after an 80-km transmission and phase-sensitive pre-amplification without CD pre-compensation by the SLM. It was confirmed that the
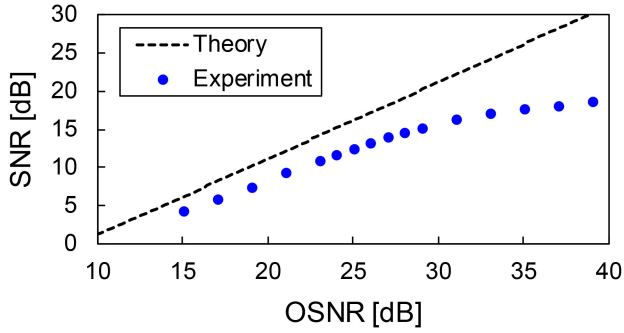
Fig. 8.   OSNR dependence of SNR after signal demodulation in 96-Gbaud SP-PS-64QAM signal.
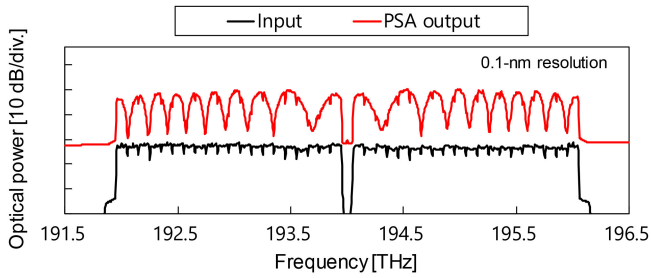

Fig. 10.   Calculated relative phase difference with respect to 194.0 THz.

Fig. 9.   Spectrum of WDM signal and its idler amplified by PSA without CD pre-compensation.
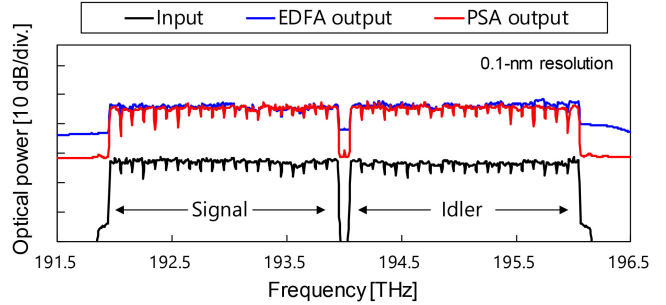
Fig. 11.   Spectra of 20-channel 96-Gbaud WDM signal pre-amplified by PSA and EDFA.

spectrum suffered from a gain ripple due to the slight residual CD in our dispersion-managed link. For accurate residual CD compensation using the SLM, we proposed a residual CD estimation method utilizing Eq. (15) [18]. Amplification and de-amplification points in the spectrum indicated the residual local CD around each point. Because a phase-sensitively amplified spectrum is very sensitive for a slight CD, a residual CD in the transmission link can be estimated accurately by measuring the output spectrum of a PSA. With the residual CD, amplification peaks and de-amplification peaks occurred in the output spectrum of a PSA at frequencies corresponded to $\Delta\phi(f) = n\pi$ and $\Delta\phi(f) = n\pi/2$, respectively. By measuring the frequencies of these peaks, the residual CD around the peaks can be calculated as follows:

$$D = \frac{f_0^2}{c\left(B_m^2 - (f_0 - f_{PLL})^2\right)} m \qquad (17)$$

$$D = \frac{f_0^2}{2c\left(B_m^2 - (f_0 - f_{PLL})^2\right)} m \qquad (18)$$

where B_m is the bandwidth between f_0 and the mth (de-)amplification peak. Equations (17) and (18) are the cases using amplification and de-amplification peaks, respectively. By feeding back the estimated CD to a SLM, the residual CD of the system can be accurately compensated, and wideband phase-sensitive amplification can be achieved. Using Eqs. (17) and (18), we estimated the residual CD distribution in the frequency domain. As shown in Fig. 5, there was a slope in the CD of the transmission link. Therefore, it was not the exact amount of CD that was estimated, but the accurate relative phase difference
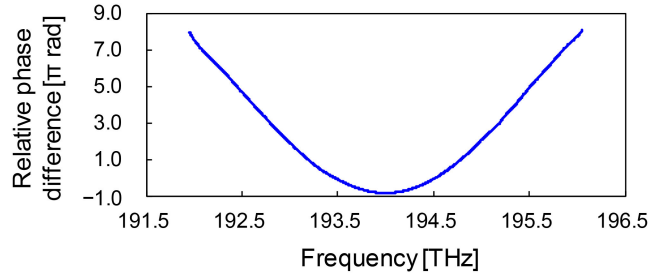
between each signal-idler pair superposed by OPA. Fig. 10 shows the estimated relative phase difference with respect to 194 THz. The averaged residual CD was +0.334 ps/nm. The CD between each point was linearly interpolated. The change from the CD in the transmission link shown in Fig. 7 was due to fiber-patch codes. On the basis of the calculated relative phase difference, we controlled the phase modulation amount of the SLM and performed CD pre-compensation.

C.   Results and Discussion

Fig. 11 shows the signal spectra pre-amplified by the PSA and the EDFA. The input spectrum was measured at the PBS input. The wideband phase-sensitive amplification over 4 THz including the idler band without gain ripples was performed thanks to the accurate CD compensation. The differences in noise floor between each pre-amplified spectrum were 8.1 dB at 191.5 THz and 8.8 dB around 194.0 THz. The PPLN-based PSA output TM-polarized ASE noise whereas the EDFA output unpolarized ASE noise. Therefore, there was a 3-dB difference in the noise floor on the measured spectrum. Considering this apparent noise difference, actual OSNR improvements by replacing the EDFA with the PSA were estimated to be about 5.1–5.8 dB depending on the frequency.

Fig. 12 shows the NGMI, SNR, and constellation diagrams of the received 20 WDM channels. In the EDFA-only case, NGMI did not exceed the FEC threshold for a net data rate of 404.72 Gbps due to the low-input power. In contrast, NGMI of all channels exceeded the threshold in the PSA case thanks to the OSNR improvements. From this result, an 8-Tbps (20 ch. × 400
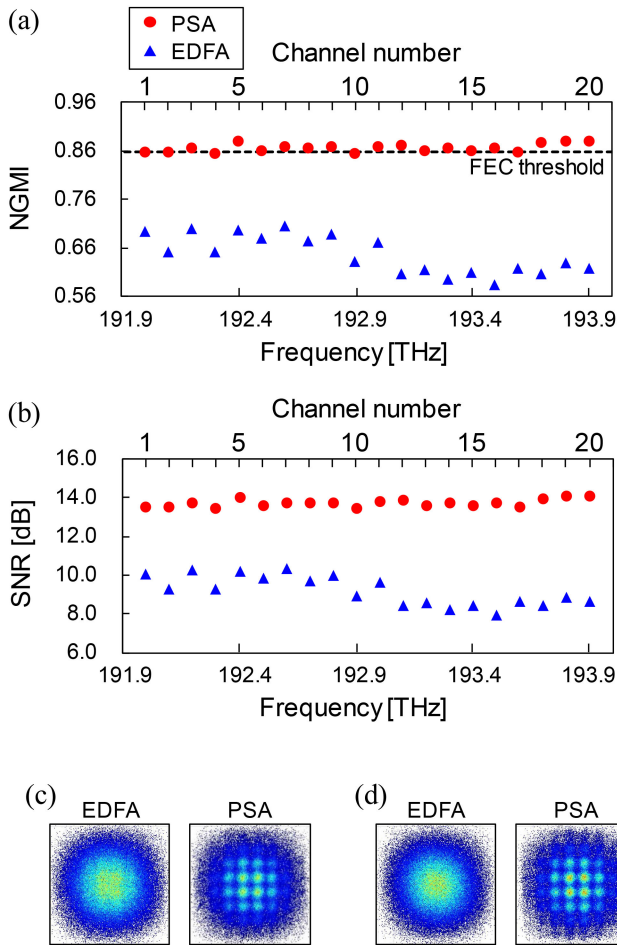
(a)

(b)

(c)

(d)

Fig. 12. Received signal characteristics. FEC threshold of NGMI was 0.857. (a) NGMI and (b) SNR of 20-ch. 96-Gbaud SP-PS-64QAM signals. Constellation diagrams of (b) ch.1 and (c) ch.20.
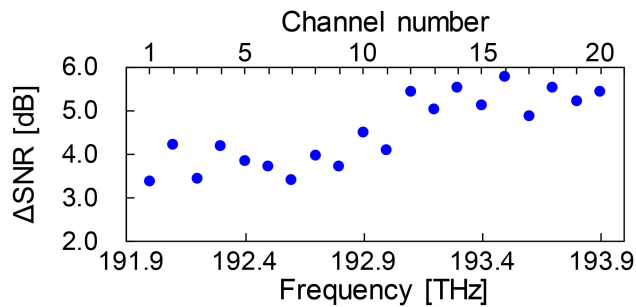

Fig. 13. ΔSNR characteristic indicates SNR improvement amount by replacing EDFA with PSA in each channel.

Gbps) transmission with the ND-PSA was successfully demonstrated. Fig. 13 shows the ΔSNR characteristics, which are the differences in SNR between the PSA/EDFA and EDFA/EDFA cases. The highest ΔSNR was 5.7 dB at ch.16 (193.5 THz). An OSNR improvement of ∼6.0 dB was estimated approximately from the OSNR-SNR characteristics of Tx/Rx shown in Fig. 8. As ch.16 was the locking point of the PZT-PLL, stable phase-sensitive amplification was performed. ΔSNR tended to

decrease as the distance from the center frequency increased. The ΔSNR at ch. 1 was 3.4 dB, and estimated OSNR improvement was ∼3.5 dB. One of the reasons for this is a mismatch of the polarization states between the signal and idler light [26]. We attempted to extract only the TM polarization with PCs, but it was difficult to perfectly match the random polarization rotation in the transmission fibers between the distant signals and idlers.

As previously mentioned, we have demonstrated an ultra-low-noise pre-amplification over 2 THz using a PPLN-based PSA. However, the launched optical power is low in our experiments. Although high fiber-launched power causes the nonlinear distortion induced by the optical Ker effect, PSA can provide mitigation of such distortion as well as low-noise amplification [6], [7]. Further benefits of wideband PSA will be evaluated by long-haul transmission experiments with longer dispersion-compensated transmission lines that can satisfy $T_{\mathrm{add}}^{-1} < 20$ dB even with high-launched optical power.

IV. CONCLUSION

We clarified a system design for a single-span transmission with phase-sensitive amplification of a high-symbol-rate and wideband WDM signal. To extend the effective range of PSAs, it is important to keep the OSNR of the signal light output from the post-amplifier high. A high-power light source and low-loss optical modulator are key technologies. In addition, we showed the impact of the quantization error in CD compensation on amplified signal quality. To extend the effective amplification band, it is necessary to apply analog CD compensation so that the residual CD is less than the specified value. We showed in numerical simulations that the residual CD needs to be <7 ps/nm to achieve a 2-THz signal amplification band when using a 1-GHz-resolution DCM.

On the basis of the aforementioned discussion, we demonstrated an 80-km single-span transmission of 20-channel 96-Gbaud SP-PS-64QAM signals using PPLN-based OPA modules as the PSA. Low-noise phase-sensitive amplification outperforming an EDFA was achieved over a 2-THz signal band thanks to the dispersion-management design in the transmission link. The transmission with a net data rate of 8 Tbps (20 × 400 Gbps/λ) was successful under a condition that could not be achieved by using an EDFA-only receiver.

REFERENCES

[1] T. Kobayashi *et al.*, "35-Tb/s C-band transmission over 800 km employing 1-Tb/s PS-64QAM signals enhanced by complex 8 × 2 MIMO equalizer," in *Proc. IEEE Opt. Fiber Commun. Conf. Exhib., OFC*, Mar. 2019, Paper Th4B.2.

[2] F. Buchali *et al.*, "1.3-Tb/s single-channel and 50.8-Tb/s WDM transmission over field-deployed fiber," in *Proc. 45th Eur. Conf. Opt. Commun.*, Sep. 2019, Paper PD.1.3.

[3] R. I. Laming, M. N. Zervas, and D. N. Payne, "Erbium-doped fiber amplifier with 54 dB gain and 3.1 dB noise figures," *IEEE Photon. Technol. Lett.*, vol. 4, no. 12, pp. 1345–1347, Dec. 1992.

[4] W. Imajuku, A. Takada, and Y. Yamabayashi, "Low-noise amplification under the 3-dB noise figure in a high gain phase-sensitive fiber amplifier," *Electron. Lett.*, vol. 35, no. 22, pp. 1954–1955, Oct. 1999.

[5] Z. Tong *et al.*, "Towards ultrasensitive optical links enabled by low-noise phase-sensitive amplifiers," *Nature Photon.*, vol. 5, no. 7, pp. 430–436, Jul. 2011.

[6] S. L. I. Olsson, B. Corcoran, C. Lundstrom, T. A. Eriksson, M. Karlsson, and P. A. Andrekson, "Phase-Sensitive amplified transmission links for improved sensitivity and nonlinearity tolerance," *IEEE J. Lightw. Technol.*, vol. 33, no. 3, pp. 710–721, Feb. 2015.

[7] K. Vijayan, B. Foo, M. Karlsson, and P. A. Andrekson, "Cross-Phase modulation mitigation in phase-sensitive amplifier links," *IEEE Photon. Technol. Lett.*, vol. 31, no. 21, pp. 1733–1736, Nov. 2019.

[8] T. Umeki *et al.*, "Polarization-diversity In-line phase sensitive amplifier for simultaneous amplification of Fiber-transmitted WDM PDM-16QAM signals," in *Proc. Opt. Fiber Commun. Conf.*, Mar. 2018, Paper M3E.4.

[9] Y. Akasaka *et al.*, "WDM amplification of one pump HNLF based phase sensitive amplifier with static pump phase tuning," in *Proc. Opt. Fiber Commun. Conf.*, Mar. 2019, Paper W4F.5.

[10] S. Shimizu *et al.*, "Optical phase-sensitive amplification of higher-order QAM signal with single Mach-Zehnder amplitude modulator," *Electron. Lett.*, vol. 57, no. 1, pp. 32–33, Jan. 2021.

[11] T. Kobayashi *et al.*, "Wide-Band inline-amplified WDM transmission using PPLN-Based optical parametric amplifier," *J. Lightw. Technol.*, vol. 39, no. 3, pp. 787–794, Feb. 2021.

[12] T. Kishimoto, K. Inafune, Y. Ogawa, H. Sasaki, and H. Murai, "Highly efficient phase-sensitive parametric gain in periodically poled $LiNbO_3$ ridge waveguide," *Opt. Lett.*, vol. 41, no. 9, pp. 1905–1908, May 2016.

[13] Y. M. Sua, J.-Y. Chen, and Y.-P. Huang, "Ultra-wideband and high-gain parametric amplification in telecom wavelengths with an optimally mode-matched PPLN waveguide," *Opt. Lett.*, vol. 43, no. 12, pp. 2965–2968, Jun. 2018.

[14] T. Kashiwazaki, K. Enbutsu, T. Kazama, O. Tadanaga, T. Umeki, and R. Kasahara, "Over-30-dB phase-sensitive amplification using a fiber-pigtailed PPLN waveguide module," in *Proc. Nonlinear Opt.*, Jul. 2019, Paper NW3A.2.

[15] T. Kazama *et al.*, "Over-30-dB gain and 1-dB noise figure phase-sensitive amplification using pump-combiner-integrated fiber I/O PPLN module," *Opt. Exp.*, vol. 29, no. 18, pp. 28824–28834, Aug. 2021.

[16] V. Gordienko, F. Ferreira, J. R. Lamb, Á. Szabó, and N. Doran, "Phase-sensitive amplification of 11 WDM channels across bandwidth of 8 nm in a fibre optic parametric amplifier," in *Proc. IEEE Eur. Conf. Opt. Commun., ECOC*, Dec. 2020, Paper Th2A-6.

[17] M. Asobe, T. Umeki, K. Enbutsu, O. Tadanaga, and H. Takenouchi, "Phase squeezing and dispersion tolerance of phase sensitive amplifier using periodically poled $LiNbO_3$ waveguide," *J. Opt. Soc. Amer. B*, vol. 31, no. 12, pp. 3164–3169, Dec. 2014.

[18] S. Shimizu *et al.*, "Accurate estimation of chromatic dispersion for non-degenerate phase-sensitive amplification," *J. Lightw. Technol.*, vol. 39, no. 1, pp. 24–32, Jan. 2021.

[19] S. Shimizu *et al.*, "8-Tbps (20 × 400 Gbps) unrepeated transmission over 80 km with 2-THz PPLN-Based phase-sensitive amplification using precise chromatic dispersion pre-compensation," in *Proc. IEEE Eur. Conf. Opt. Commun., ECOC*, Sep. 2021, Paper Tu4C1.4.

[20] S. L. I. Olsson *et al.*, "Injection locking-based pump recovery for phase-sensitive amplified links," *Opt. Exp.*, vol. 21, no. 12, pp. 14512–14529, Jun. 2013.

[21] Y. Okamura *et al.*, "Optical pump phase locking to a carrier wave extracted from phase-conjugated twin waves for phase-sensitive optical amplifier repeaters," *Opt. Exp.*, vol. 24, no. 23, pp. 26300–26306, Nov. 2016.

[22] Z. Tong, C. Lundström, P. A. Andrekson, M. Karlsson, and A. Bogris, "Ultralow noise, broadband phase-sensitive optical amplifiers, and their applications," *IEEE J. Sel. Top. Quantum Electron.*, vol. 18, no. 2, pp. 1016–1032, Mar./Apr. 2012.

[23] M. Roelens, J. Schröder, P. Blown, C. Pulikkaseril, S. Poole, and S. Frisken, "Applications of LCoS-Based programmable optical processors," in *Proc. Opt. Fiber Commun. Conf.*, Mar. 2014, Paper W4F.3.

[24] W. Imajuku and A. Takada, "Noise figure of phase-sensitive parametric amplifier using a Mach-Zehnder interferometer with lossy Kerr media and noisy pump," *IEEE J. Quantum Electron.*, vol. 39, no. 6, pp. 799–812, Jun. 2003.

[25] T. Kazama, T. Umeki, M. Abe, K. Enbutsu, Y. Miyamoto, and H. Takenouchi, "Low-parametric-crosstalk phase-sensitive amplifier for guard-band-less DWDM signal using PPLN waveguides," *IEEE J. Lightw. Technol.*, vol. 35, no. 4, pp. 755–761, Feb. 2017.

[26] A. L.-Riesgo, P. A. Andrekson, and M. Karlsson, "Polarization-Independent phase-sensitive amplification," *IEEE J. Lightw. Technol.*, vol. 34, no. 13, pp. 3171–3180, Jul. 2016.

Shimpei Shimizu (Member, IEEE) received the B.E. degree in engineering and the M.E. degree in information science and technology in the field of electronics for informatics from Hokkaido University, Sapporo, Japan, in 2016 and 2018, respectively. In 2018, he joined NTT Network Innovation Laboratories, Yokosuka, Japan. His research focuses on high-capacity optical transmission systems. He is a Member of the Institute of Electronics, Information and Communication Engineers of Japan and the IEEE Photonics Society. He was the recipient of the 2017 IEICE Communications Society Optical Communication Systems Young Researchers Award.

Takayuki Kobayashi (Member, IEEE) received the B.E., M.E., and Dr. Eng. degrees from Waseda University, Tokyo, Japan, in 2004, 2006, and 2019, respectively. In April 2006, he joined NTT Network Innovation Laboratories, Yokosuka, Japan, where he was engaged in the research on high-speed and high-capacity digital coherent transmission systems. In April 2014, he moved to NTT Access Network Service Systems Laboratories, Yokosuka, Japan, and was engaged in 5G mobile optical network systems. Since July 2016, he moved back to NTT Network Innovation Laboratories and has been working on high-capacity optical transmission systems. His current research interests include long-haul optical transmission systems employing spectrally efficient modulation formats enhanced by digital and optical signal processing. He is a Member of the Institute of Electronics, Information and Communication Engineers of Japan. From 2016 to 2018, he was a Technical Program Committee (TPC) Member of the Electrical Subsystems' Category for the Optical Fiber Communication Conference. Since 2018, he has been a TPC Member of the Point-to-Point Optical Transmission Category for the European Conference on Optical Communication.

Takushi Kazama received the B.S. and M.S. degrees in electrical engineering from The University of Tokyo, Tokyo, Japan, in 2009 and 2011, respectively. In 2011, he joined NTT Device Technology Laboratories, Japan, where he has been engaged in research on nonlinear optical devices based on periodically poled $LiNbO_3$ waveguides. He is a Member of the Institute of Electronics, Information, and Communication Engineers of Japan and Japan Society of Applied Physics.

Takeshi Umeki (Member, IEEE) received the B.S. degree in physics from Gakusyuin University, Tokyo, Japan, in 2002, and the M.S. degree in physics and the Ph.D. degree in nonlinear optics from The University of Tokyo, Tokyo, Japan, in 2004 and 2014, respectively. In 2004, he joined NTT Photonics Laboratories, Atsugi, Japan, since then he has been involved in research on nonlinear optical devices based on periodically-poled $LiNbO_3$ waveguides. He is a Member of the Japan Society of Applied Physics, Institute of Electronics, Information, and Communication Engineers, and IEEE/Photonics Society.

Masanori Nakamura (Member, IEEE) received the B.S. and M.S. degrees in applied physics from Waseda University, Tokyo, Japan, in 2011 and 2013, respectively, and the Ph.D. degrees in electrical, electronic, and infocommunications engineering from Osaka University, Osaka, Japan, in 2021. In 2013, he joined NTT Network Innovation Laboratories, Yokosuka, Japan, where he engaged in research on high-capacity optical transport networks. He is a Member of the Institute of Electronics, Information and Communication Engineers, Tokyo, Japan. He was the recipient of the 2016 IEICE Communications Society Optical Communication Systems Young Researchers Award.

Koji Enbutsu received the B.E. and M.E. degrees in electronics engineering from Hokkaido University, Sapporo, Japan, in 1994 and 1996, respectively. In 1996, he joined NTT Opto-Electronics Laboratories, Japan, where he engaged in research on organic optical waveguides for optical communications and electro-optic crystals and their devices. In 2007, he moved to NTT Access Services Network System Laboratories, where he engaged in research on optical fiber testing and monitoring. He is a Member of the Institute of Electronics, Information, and Communication Engineers and Japan Society of Applied Physics.

Ryoichi Kasahara received the B.S. degree from The University of Electro-Communications, Tokyo, Japan, in 1995, and the M.S. degree from Tohoku University, Sendai, Japan, in 1997. In 1997, he joined NTT Opto-Electronics Laboratories, Japan, where he was involved in research on silica-based planar lightwave circuits, including thermo-optic switches and arrayed-waveguide grating multiplexers, and integrated optoelectrical receiver modules. He is currently with NTT Device Technology Laboratories, Japan, where he has been involved in the research and development of the fabrication technologies of optical dielectric waveguide devices. He is a Senior Member of the Institute of Electronics, Information, and Communication Engineers of Japan and a Member of the Japan Society of Applied Physics.

Yutaka Miyamoto (Member, IEEE) received the B.E. and M.E. degrees in electrical engineering from Waseda University, Tokyo, Japan, in 1986 and 1988, respectively, and the Dr. Eng. degree in electrical engineering from Tokyo University, Tokyo, Japan, in 2016. In 1988, he joined NTT Transmission Systems Laboratories, Yokosuka, Japan, where he was engaged in the research and development of high-speed optical communications systems, including the 10-Gbit/s first terrestrial optical transmission system (FA-10G) using erbium-doped fiber amplifiers inline repeaters. From 1995 to 1997, he was with NTT Electronics Technology Corporation, Yokohama, Japan, where he was engaged in the planning and product development of high-speed optical module at the data rate of 10 Gb/s and beyond. Since 1997, he has been with NTT Network Innovation Laboratories, Yokosuka, Japan, where he has contributed to the research and development of optical transport technologies based on 40/100/400-Gbit/s channel and beyond. He is currently an NTT Fellow and the Director of the Innovative Photonic Network Research Center, NTT Network Innovation Laboratories, where he has been investigating and promoting the future scalable optical transport network with the Pbit/s-class capacity based on innovative transport technologies, such as digital signal processing, space division multiplexing, and cutting-edge integrated devices for photonic preprocessing. He is a Fellow of the Institute of Electronics, Information and Communication Engineers.